Human bone marrow adipocytes drive prostate cancer bone metastasis progression via lipid-mediated induction of Angiopoietin-like 4

Marine Hernandez[1,2], Sauyeun Shin[1,2], David Rengel[1], Stéphanie Dauvillier[1,2], Nancy Geoffre[3,4], Carine Valle[5], Alessandro Taccini[1,2] Mohamed Moutahir[1,2], Justine Bertrand-Michel[3,4], Nicolas Reina[6,7], Catherine Muller[1,2*] and Camille Attané[1,2*].

[1] Institut de Pharmacologie et de Biologie Structurale (IPBS), Université de Toulouse, CNRS, Toulouse, France.
[2] Equipe Labellisée Ligue Contre Le Cancer, Toulouse, France.
[3] MetaboHUB-MetaToul, National Infrastructure of Metabolomics and Fluxomics, Toulouse, 31077, France.
[4] Université de Toulouse, Inserm, I2MC, Toulouse, France.
[5] Université de Toulouse, Inserm, CRCT, Toulouse, France.
[6] Département de Chirurgie Orthopédique et Traumatologique, Hôpital Pierre-Paul Riquet, CHU de Toulouse, Toulouse, France.
[7] Laboratoire AMIS, UMR 5288 CNRS, Université de Toulouse Toulouse, France.
* Correspondence: muller@ipbs.fr and camille.attane@ipbs.fr

Abstract

Bone is the main metastatic site in advanced prostate cancer (PCa) and contains bone marrow adipocytes (BMAds), which account for more than 70% of adult bone marrow. However, their role in the progression of PCa metastases remains poorly understood. Herein, we developed a physiologically relevant 3D culture model using primary human BMAds from red hematopoietic rich-areas (rBMAds) and we showed that rBMAds engage in metabolic crosstalk with PCa cells. Specifically, rBMAds release free fatty acids (FFAs) through a non-canonical lipolytic pathway and these FFAs are taken up by PCa cells inducing a transcriptional reprogramming that promotes motility. Among the responsive genes, Angiopoietin like 4 (ANGPTL4) is the most upregulated via a peroxisome proliferator-activated receptor γ-dependent mechanism, and its silencing abolishes the rBMAd-driven migratory and invasive phenotype. In bone metastases of patients with PCa, high ANGPTL4 levels correlate with poor survival. Together, our findings uncover a novel adipocyte-tumor interaction and identify ANGPTL4 as a key mediator and potential therapeutic target in bone-metastatic PCa.

Key words

Prostate cancer metastases, primary human bone marrow adipocytes, metabolic crosstalk, lipids, migration, ANGPTL4

Introduction

Prostate cancer (PCa) is the second most commonly diagnosed cancer and the fifth leading cause of cancer-related death among men worldwide[1,2]. While many patients benefit from curative therapies, approximately one-third progress to advanced metastatic disease, which remains a major life-limiting condition[3,4]. Among distant metastases, the bone is the predominant site of colonization, with nearly 80% of advanced PCa patients developing bone lesions, predominantly osteoblastic metastases[4–6]. The bone microenvironment supports metastatic establishment, progression and resistance to therapy, involving a complex interplay among osteoblasts, osteoclasts, stromal and immune cells and the extracellular matrix[7,8]. Despite their proximity to PCa bone metastases, bone marrow adipocytes (BMAds) remain one of the most abundant yet understudied components of the metastatic bone niche[9]. As metabolically active and secretory cells, BMAds are known to regulate normal hematopoiesis, bone remodeling and onset of hematologic malignancies, primarily based on evidence from preclinical models[9,10]. However, their role in PCa bone metastasis remains poorly defined.

Growing evidence, including our own, strongly supports the idea that adipocyte–tumor cell interactions, particularly metabolic exchanges, play a pivotal role in cancer, including PCa progression.

At the primary tumor site, periprostatic adipose tissue (PPAT), a white adipose tissue (WAT) surrounding the prostate[11], contributes to PCa progression through paracrine mechanisms[12]. While soluble factors such as chemokines and pro-inflammatory cytokines from PPAT have been shown to enhance PCa aggressiveness and local dissemination[12,13], a more specific and increasingly recognized mechanism involves the direct transfer of free fatty acids (FFAs) from adipocytes to tumor cells[14]. Tumor cells induce FFA release from adipocytes by activating lipolysis, a major metabolic pathway in adipocytes that involves the hydrolysis of triglycerides (TGs) into FFAs and glycerol[15,16]. In turn, these FFAs are taken up by cancer cells and exploited for their own advantage[16]. This form of metabolic symbiosis is now recognized across multiple cancer types including melanoma, ovarian, breast, and colon cancers[16]. Depending on the tumor type, FFAs taken up by cancer cells can act directly as substrates for a range of pathways, including fatty acid β-oxidation (FAO), signaling and transcriptional remodeling or be converted into neutral lipids (mainly, TGs) and stored in lipid droplets (LDs) to avoid lipotoxicity[16]. In PCa, at the primary tumor site, we have shown that FFA uptake induces expression of the pro-oxidant enzyme NADPH oxidase 5 (NOX5), triggering signaling cascades that promote tumor invasion[14]. Therefore, the fate of lipids in tumor cells depends both on the tumor type and the nature of the proximal adipose depot. Understanding the mechanisms and consequences of lipid transfer from adipocytes to tumor cells is essential in the context of PCa metastasis to lipid-rich environments such as the bone marrow. The dynamic interplay between tumor

cells and adipocytes represents not only a critical axis in cancer progression but also a potential therapeutic target that remains largely underexplored in the field of PCa metastasis.

Accumulating evidence indicates that BMAds exhibit specific metabolic and functional properties that differ markedly from other "classical" adipocytes[9,10]. Two distinct adipocyte populations exist in rodents : constitutive bone marrow adipocytes (cBMAds), located in areas devoid of hematopoietic cells and resistant to metabolic cues, and regulatory BMAds (rBMAds), interspersed within hematopoietic niches and responsive to energy stress and other signals, likely via lipolysis[9,10] at least in rodents. Using femoral bone marrow aspirate of patients undergoing hip replacement surgery[17], we have demonstrated that in humans, both types of adipocytes lack lipolytic activity[18,19]. Furthermore, we recently demonstrated that rBMAds, frequently found in proximity to metastatic lesions[20], are anucleate but maintain metabolic and secretory functions that support hematopoiesis *in vitro*[19]. In both acute myeloid and lymphoblastic leukemias, which occur in areas of active hematopoiesis, a decrease in the number and size of rBMAds is observed, highlighting that dynamic remodeling of rBMAds also occurs in humans[21]. One very important point that needs to be underlined from our studies is that the metabolic specificity of human primary BMAds, particularly their altered lipolysis, is not recapitulated in *in vitro*–differentiated adipocytes, derived from preadipocyte cell lines or human bone marrow mesenchymal stem cells (BM-MSCs)[18]. Cocultures of *in vitro* differentiated adipocytes and PCa cell lines have demonstrated that lipid transfer occurs[22], driven by adipocytes lipolysis[23,24], leading to increased invasion, enhanced survival, and chemoresistance of PCa cells[23,25]. However, as stated below, since these models fail to recapitulate the metabolic characteristics of primary BMAds[18], these results should be interpreted with caution. The use of primary human rBMAds, which is essential for investigating their involvement in cancer progression, has been limited to date by technical challenges associated with their isolation, anatomical localization, and the difficulty of maintaining them in culture for *in vitro* studies[26].

To overcome these limitations, we developed a three-dimensional culture model of primary human rBMAds isolated from the femoral bone marrow of patients undergoing hip surgery. This model preserves rBMAds viability and metabolic function and reveals a previously unrecognized metabolic crosstalk in which rBMAds release FFAs via a non-canonical lipolytic mechanism. These FFAs are taken up by PCa cells, inducing a transcriptional program that promotes motility and invasion. We further identify angiopoietin-like 4 (ANGPTL4) as a peroxisome proliferator-activated receptor γ (PPARγ)-dependent effector of FFA signaling. Extending our previous findings that rBMAds promote PCa bone homing[27], we show here that they also enhance PCa cell motility and invasion. Together, these data suggest that rBMAds facilitate both bone colonization and subsequent metastatic dissemination, positioning ANGPTL4 as a potential therapeutic target in advanced PCa.

Materials and Methods

Collection of adipose tissue samples and adipocyte isolation

BMAT and subcutaneous adipose tissue (SCAT) were harvested from patients undergoing hip surgery at the Orthopedic Surgery and Traumatology Department of the Hospital Pierre Paul Riquet (Toulouse, France) as previously reported[18]. All patients gave informed consent and the samples were obtained according to national ethics committee rules (authorization DC-2019-3784). For all experiments, samples were obtained from 123 men and 27 women (mean age: 67.6 years and mean body mass index (BMI): 25.1kg/m^2). All patient information's are summarized in Table S1. Woman samples were used only for the development of rBMAd 3D culture model, lipolysis experiments and for the quantification of FFA and glycerol release by rBMAds cultured in BSA medium.

After obtention, the samples were immediately placed in 37°C pre-warmed KRBHA (Krebs Ringer Buffer HEPES Albumin buffer) corresponding to Krebs Ringer buffer (Sigma-Aldrich) supplemented with 100mM HEPES (Sigma-Aldrich) and 0.5% FFA-free bovine serum albumin (BSA) (Sigma Aldrich) at pH 7.4 and rapidly transferred to the laboratory (within 1h) where they were processed. Subcutaneous adipocytes (SCAds) from SCAT and rBMAds from "red" BMAT were isolated as we previously described[19]. Briefly, SCAT was digested with collagenase (250 UI/ mL) diluted in calcium and magnesium free PBS supplemented with 2% FA-free BSA during and 30 minutes at 37°C under constant shaking and samples were filtered with 200µm cell strainers. For BMAT, "red" BMAT was directly filtered with 100µm cell strainer and floating rBMAds were collected. SCAds and rBMAds were washed several times with KRBHA until a clear suspension was obtained. For rBMAds, a centrifugation at 300 g for 5 minutes at room temperature (RT) was performed to remove cell debris and obtain pure cell suspension.

3D culture and preparation of conditioned medium (CM) of rBMAds

Fibrin gels of SCAds and rBMAds were performed as previously described[28]. Briefly, 70µL of fibrinogen at 18mg/mL (Sigma Aldrich F8630-5G) in NaCl 0.9% (4.2mg/mL final concentration) were mixed with 1.5µL or 7µL of aprotinin (Sigma Aldrich A1153) at 5mg/mL (25µg/mL and 110µg/mL final concentration for 3 days and 5 days of coculture respectively) and 30µL of PBS-$CaCl_2$ in 2mL eppendorf tube. One hundred microliters of SCAds or rBMAds were added and homogenized quickly with 100µL of thrombin 25UI/mL (Sigma Aldrich T6634-1KU) in PBS-$CaCl_2$ (8.3UI/mL final concentration). After gel polymerization, gels were transferred in 12-well plates, containing 2.5mL of medium, to be cultivated alone or in coculture with PCa cell lines.

To validate the 3D culture model, a suspension of 50µL of rBMAds were included in fibrin gel and fixed with paraformaldehyde 3.7% during 20 minutes. Cells were then stained with BODIPY® 493/503 (for neutral lipids) at 1µg/mL. For each adipocyte sample, at least 3 images were acquired with LSM710 confocal microscope (Zeiss). Cell diameter measurement was performed manually using ImageJ/Fiji® software (Image J, Bethesda, MD, USA). For the quantification of adiponectin secretion overtime, rBMAds gel was incubated during 3h in RPMI without FBS at day 1, day 2 and day 3 of culture at 37°C in a humidified atmosphere with 5% CO_2. Medium were cautiously collected and centrifuged at 500g for 5 minutes at RT to eliminate cell debris. The quantification of adiponectin was realized with Human DuoSet ELISA kits from R&D Systems (#DY1065-05) according to the manufacturer's instruction.

To performed conditioned medium (CM) of rBMAds, fibrin gels were incubated in 1mL of RPMI (ThermoFisher Scientific #11879020) without FBS and supplemented with 5mM of glucose and 0.5% BSA (Sigma Aldrich). After 3 days of incubation, at 37°C in a humidified atmosphere with 5% CO_2, CM were collected, centrifuged at 300g for 5 minutes at RT to remove cellular debris. CM were stored at -20°C until treatment with PCa cell lines. Delipidated CM (dCM) were prepared with Cleanascite™ lipid removal reagent (Gentaur, #0337-X2555-10) at ratio 1 :1. Samples were gently shaken for 20 minutes, followed by 10 minutes of centrifugation at 5000g and the supernatant was used as dCM.

Cell line culture and coculture

The human PCa cell lines, PC3 (ATCC CRL-1435), LNCaP (ATCC CRL-1740) and Du145 (ATCC HTB-81) were used in this study and derived from bone, lymph node and brain metastasis respectively. PC3 and LNCaP were cultivated in RPMI medium (ThermoFisher Scientific # 11879020) supplemented with 5mM glucose (Sigma Aldrich), 5% FBS (Foetal Bovine Serum) and 1% Penicillin–Streptomycin (P/S). Du145 cells were cultivated in RPMI GlutaMAX™ medium (ThermoFisher Scientific #61870044) supplemented with 10% FBS and 1% P/S. Cells were grown at 37°C, in a humidified atmosphere with 5% CO_2 and used within 2 months after resuscitation of frozen aliquots. The cells were tested every month by polymerase chain reaction for mycoplasma contamination.

For coculture experiments, PCa cell lines were seeded at 10 000 cells/well for PC3 and 30 000 cells/well for Du145 and LNCaP in 12-well plates. For confocal microscopy, PCa cell lines were seeded on a coverslip. One day after seeding, medium was replaced by 2.5mL of fresh medium and rBMAds gel were added in a well and float above tumor cells. For the direct transfer of fluorescent palmitate (BODIPY™ FL-C16, Fisher #D3821), rBMAds suspension were loaded during 4 hours with 5µM of BODIPY™ FL-C16 prior to be embedded in fibrin gel and used for coculture with PCa cells.

Lipolysis assay

Lipolysis activity was performed as we previously described[18,19]. Briefly, SCAds and rBMAds in suspension were incubated for 3 hours at 37°C in KRBHA with or without isoproterenol 1µM(Sigma Aldrich, #I6504) or forskolin 10µM (Sigma Aldrich, #F6886) to evaluate stimulated and basal lipolysis. For experiments with lipase inhibitors, suspension of isolated SCAds and rBMAds were preincubated 1 hour at 37°C with or without 100µM orlistat (Sigma Aldrich #O4139) or 100µM paraoxon ethyl (Sigma Aldrich #D9286) before adding isoproterenol 1µM. At the end of the incubation, media were collected to measure glycerol and FFA release using commercial kits (Sigma F6428 and Wako diagnostic NEFA-HR, respectively). Absorbance was read at a wavelength of 550nm and 540 nm for FFA and glycerol respectively according the manufacturer's instructions.

FFA release and neutral lipid quantification

PC3 alone (NC), rBMAds alone (rBMAds NC) or PC3 cultivated with rBMAds (COC) were incubated during 72 hours in 12-well plates in medium containing 5% FBS or 0.5% BSA depending on the experiment. Medium were then centrifuged for 5 minutes at 300g at RT to remove any cellular debris. FFA and glycerol released into medium were measured as described above. For FFA species quantification, lipids were extracted from the medium of rBMAds NC, PC3 NC and COC and analyzed as we previously described[19].

For evaluation of TG content, tumors cells cultivated or not with rBMAds were lyzed in TE 1X buffer (10 mM Tris-HCl, 1 mM EDTA, pH 7.5) and TG content was quantified using a Triglyceride reagent (Sigma, Aldrich) according the manufacturer's instructions. The results were normalized by the concentration of protein evaluated by BCA Assay (Biorad). For neutral lipid quantification of PC3 NC and COC, lipids were extracted according to Bligh and Dyer[29] in CH_2Cl_2:MeOH :water (2.5:2.5:2, v/v/v) in the presence of the internal standards. Organic phase was dried and dissolved in 20 µL of ethyl acetate. 1 µL of the lipid extract was analyzed by gas chromatography flam ionization detector on a GC TRACE 1300 Thermo Electron system using an RTX-5 column (Restek). Oven temperature was programmed from 210°C to 350°C at a rate of 5°C/min and the carrier gas was hydrogen (5ml/min). The injector and the detector were at 315°C and 345°C respectively. Finally, peak detection, integration and relative quantitative analysis were done using Chromeleon 7.3.1 (Thermo Scientific).

Cell line treatments

For exogenous FFA treatment, PCa cell lines were seeded at 10 000 cells/well for PC3 and 30 000 cells/well for Du145 and LNCaP in 12 well-plates and at 2000 cells/well for PC3 in 96 well-plates. One

day after seeding, cells were treated with 100µM palmitate (Cayman #29558), 100µL oleate (Sigma Aldrich #O3008), 100µM linoleate (Sigma Aldrich #L9530), or with the mix of 3 FFAs (100µM palmitate/100µM oleate/100µM linoleate) during 3 days.

For PPARγ inverse agonist treatment, PC3 and Du145 were seeded at 10 000 cells/well and 30 000 cells/well in 12 well-plates respectively. Three days after seeding, cells were preincubated during 1h with T0070907 10µM (Cayman #10026) followed by exogenous FFA treatment for 24h at the same concentration mentioned above or by coculture with rBMAds for 24h.

Boyden chamber migration and invasion assay

After coculture, CM treatment or exogenous FFA treatment, 50 000 cells, were seeded in 8.0µm Transwells (Corning, #353097) placed in 24-well plates for migration assay. For invasion assay, Matrigel (Corning, #356231) was diluted 1:80 and 150 000 cells were seeded on the top of Matrigel contained in 8.0µm Transwells (Corning, #353182) placed in 12-well plates. The lower chamber was filled with RPMI (ThermoFisher Scientific) without serum (used as control) or containing 10% FBS. After 24h of migration or invasion, non-migrated cells were removed with a cotton swab except for a control assay to evaluate the total number of cells at the end of the experiment. Migratory cells were fixed in methanol and stained with Toluidine Blue 1% supplemented with 0.1M borax (Sigma). Transwell membranes were cut and incubated in a lysis buffer (Tris HCl 6.25mM pH 6.8, Glycerol 10%, SDS 2% and β-mercaptoethanol 5%). Absorbance was measured at 570nm and the percentage of migration and invasion is determined with migrating cells and the total number of cells.

Scratch assay

After coculture or exogenous FFA treatment for 72 hours, cells are confluent and a wound was realized with a tip for 12 well-plate (coculture condition) or with IncuCyte® WoundMaker Tool for 96-well plate (treatment with exogeneous FFA). Medium was changed to remove cellular debris. Plates were imaged during 24h, every hour, with IncuCyte® live-cell imaging system. Wound closure was determined with IncuCyte® software for 96-well plate and with ImageJ/Fiji® plugin *Wound Healing Size Tool* for 12 well-plates. Wound healing was normalized to the initial wound.

Proliferation assay

PC3, Du145, LNCaP NC and COC were counted with Malassez hemocytometer at 24, 48 and 72 hours of coculture. Proliferation was also evaluated by BrdU assay for PC3. Briefly, cells were then incubated 24h with BrdU and the proliferation is evaluated according to the manufacturer's protocol (Cell Signaling, Cat. #6813) each day during 72 hours.

short interfering RNA (siRNA) transfection

PC3 and Du145 were transiently transfected with ANGPTL4 siRNA pool (final concentration 25nmol/L) using ON-TARGETplus SMARTpool (Thermo Scientific Dharmacon) or ON-TARGETplus nontargeting pool used as a control (Thermo Scientific Dharmacon). Transfection was done according to the manufacturer's instructions with Lipofectamine RNAiMAX (Invitrogen Life Technologies) followed by 24h of coculture with rBMAds. After coculture, a second transfection was done and gene extinction, migration and invasion were evaluated. The sequences of the four siRNA against ANGPTL4 are 5′ GGAGACAUCCUUCCGCAAA 3′; 5′GAUGGGAUCUGCACUGUAA 3′; 54GAAAUUAGGUCUGGGGAUA 3′ and 5′GCAGGAAGGACCUCUAGAA 3′.

RNA extraction and quantitative real-time PCR

PC3 and Du145 NC and COC were trypsinized and centrifuged for 5 minutes at 800g at 4°C and washed 3 times with PBS. RNA extraction was performed on pellets using the RNeasy® Mini kit columns (Qiagen) following the manufacturer's instructions. Gene expression was quantified by quantitative real-time PCR (ANGPTL4: Hs01101123_g1) with TaqMan primers with a CFX96 real time PC3 system (BioRad). Results were normalized with 18S rRNA (Hs99999901_s1).

RNA sequencing (RNA-seq)

RNA was extracted as described above. RNA was quantified by Qubit RNA kit (Thermofischer Scientific) and qualified with the HS RNA kit for the Fragment Analyzer (Agilent Technologies). The mRNAseq libraries were prepared with the Illumina Stranded mRNA Prep Ligation kit using an input of 500ng of high-quality RNA (RQN =10) following manufacturer's instructions. The libraries were profiled with the HS NGS kit for the Fragment Analyzer and quantified by qPCR using the KAPA library quantification kit (Roche Diagnostics), pooled and sequenced on the Illumina NextSeq550 High Output flow cell 150 cycles. The dual-indexed sequencing parameters were 74, 10, 10, 74 cycles (read 1, index i7, index i5, read 2). Sequencer output files have been demultiplexed with the Illumina's software bcl2fastq. Reads were mapped to the annotated Homo sapiens genome (GRCh38v97) using bowtie2 aligner (v2.4.4)[30]. RSEM software (v1.3.3)[31] was used to quantify the gene expression. Statistical analysis and visualization were carried out in R working environment[32] using the RStudio interface[33]. Data wrangling and visualization were carried out using the Tidyverse meta-package[34]. RNA-seq data analysis was performed using the edgeR package[35]. Genes with a sufficient number of reads were considered as differentially expressed when their Bonferroni-corrected p-value obtained

from Quasi-Likelihood F-Test was inferior to 0.05. Gene Ontology analysis were completed using the clusterProfiler package[36]. R source codes are available upon request.

ELISA ANGPTL4

Culture medium and PCa cells were collected after 24 and 72 hours of culture of rBMAds NC, PCa NC and COC with or without siANGPTL4 transfection. The quantification of intracellular ANGPTL4 and ANGPTL4 secretion is performed with Human ANGPTL4 ELISA kit (HUES01556, Ozyme) according to the manufacturer's protocol.

Confocal microscopy on PCa cell lines

After coculture or exogenous FFA treatment, PCa cells were fixed with paraformaldehyde 3.7% during 20 minutes at RT. Cells were then stained with BODIPY® 493/503 (for neutral lipids) at 2.5 ng/mL, with rhodamine-phalloidin 1:1000 (for actin cytoskeleton) (Abcam) and with DAPI (for nucleus) at 1µM (Thermo Fisher Scientific) as previously described[28]. Fluorescence images were acquired with a confocal microscope (LSM710, Zeiss International, Germany) and analyzed with ImageJ/Fiji® software.

Survival analysis

Clinical data and RNA expression levels of ANGPTL4 were retrieved from the *Metastatic Prostate Adenocarcinoma (SU2C/PCF Dream Team, PNAS 2019)* cohort available on cBioportal (http://www.cbioportal.org) which includes 26 bone metastases PCa patients. Patients were classified into two groups based on ANGPTL4 expression level: low expression (<5 FPKM) and high expression (>5 FPKM). We compared the patients with the lowest and the highest expression of ANGPTL4 and performed survival analysis. P value was generated by using log-rank test. This dataset corresponds to the study published by Abida et al. (2019) in Proceedings of the National Academy of Sciences[37].

Statistical analyses

Data correspond to the mean ± standard error of the mean (S.E.M) of independent experiments. Statistical analysis was carried out using the Student's t test, one-way ANOVA or two-way ANOVA depending on the experiments (details in figure legends). The Tukey or Sidak correction was applied for one-way ANONVA and 2-way ANOVA. *, **, *** and **** in the figures refer to statistical probabilities (P) of <0.05, <0.01, <0.001 and <0.0001, respectively. GraphPad Prism 10.6 software was used for all the statistical analyses.

Results

Transfer of FFA is observed between rBMAds and PCa cells in a 3D co-culture model

To investigate the potential metabolic crosstalk between primary human rBMAds and PCa cells, we developed a 3D co-culture model that maintains rBMAds viability and function over time (Supplementary Fig.1). Due to their buoyancy, rBMAds lyse rapidly in 2D culture, as other adipocytes. To overcome this limitation, we adapted a 3D fibrin-matrix model previously developed for mammary adipocytes[28]. This model provides the dual advantage of preserving adipocyte viability for 3–5 days and enabling co-culture with tumor cells without compromising the integrity of the matrix[28].

Primary rBMAds isolated from BMAT were embedded in a 3D fibrin matrix. The morphology and size of the adipocytes were monitored for up to 5 days using BODIPY 493/503 staining (Supplementary Fig. 1A-B). Confocal microscopy revealed that rBMAds were homogeneously distributed within the matrix and maintained their spherical morphology (Supplementary Fig. 1A) and size (Supplementary Fig. 1B) over time. Adiponectin secretion also remained stable (Supplementary Fig. 1C). Together, these results demonstrate that the 3D fibrin matrix effectively maintains rBMAds morphology, size and function over time.

To assess metabolic interactions between rBMAds and PCa cells, PC3 cells were co-cultured (COC) or not (NC) with rBMAds for 72 hours. Unlike PC3 NC, PC3 COC accumulated numerous neutral lipid-containing LDs over time, visible as early as 24 hours post-co-culture and displayed morphological modifications (Fig. 1A). This phenotype was replicated in two additional PCa cell lines, Du145 and LNCaP (Supplementary Fig. 2A). Lipidomic profiling of PC3 cells after 72 hours of co-culture revealed a marked increase in TG content, while cholesteryl ester (CE) levels showed a modest increase, and free cholesterol (FC) levels remained unchanged (Fig. 1B). These findings were corroborated in the Du145 and LNCaP cell lines (Supplementary Fig. 2B).

To directly trace FFA transfer from rBMAds to tumor cells, we used a pulse-chase assay previously established by our group[38]. rBMAds were preloaded with BODIPY FL-C16, a fluorescently labeled saturated FA (palmitate), and then co-cultured with PC3 for up to 72 hours. Fluorescent LDs increased in PC3 between 24 and 72 hours (Fig. 1C), indicating FFA transfer, which was further confirmed by flow cytometry (Fig. 1D). These data collectively demonstrate that PCa cells can trigger the release of FFAs from rBMAds cultured in 3D, which are then rapidly taken up and re-esterified into TGs by cancer cells.

To further characterize this metabolic crosstalk, we quantified the composition of FFAs in the culture medium of PC3 NC, PC3 COC or rBMAds cultured alone (Fig. 1E). At baseline, rBMAds primarily released oleate (C18:1n7), palmitate (C16:0), and linoleate (C18:2n6), consistent with human adipose tissue FFA profiles, where these three FFAs comprise ~85% of total TGs[39]. In co-culture, the levels of these FFAs tended to increase (Fig. 1E), a trend also observed in total FFA content (Fig. 1F). However, these changes did not reach statistical significance, likely reflecting the dynamic balance between FFA release from rBMAds and uptake by PCa cells in the co-culture system.

In summary, these results demonstrate for the first time a direct metabolic crosstalk between primary human rBMAds and PCa cells. Notably, despite their absence of lipolytic activity upon β-adrenergic simulation[19], rBMAds can be induced by PCa cells to release FFAs via a mechanism yet to be elucidated.

rBMAds exhibit non-canonical lipolysis with uncoupled FFA and glycerol release

We previously demonstrated that both human cBMAds and rBMAds lack canonical lipolytic activity[18,19]. Canonical lipolysis involves catecholamine-mediated stimulation of TG hydrolysis, through sequential activation of three lipases, and release of glycerol and FFAs[15] (Fig. 2A). To test their lipolytic activity, isolated rBMAds and SCAds (used as controls) were treated with isoproterenol (ISO, a β-adrenergic agonist) or forskolin (FK, an adenylyl cyclase activator) for 3 hours. As previously reported[19], rBMAds released minimal glycerol at baseline compared to SCAds, and this release was not enhanced by ISO or FK treatment (Fig. 2B). Moreover, while basal FFA release was comparable between rBMAds and SCAds, only SCAds significantly increased FFA release following lipolytic stimulation (Fig. 2B). These findings confirm that rBMAds do not undergo complete lipolysis, as evidenced by their inability to release glycerol under basal and stimulated conditions, but they displayed FFA release independent of glycerol, suggesting the presence of a non-canonical mechanism. To further investigate this hypothesis, we extended the incubation time to 72 hours in the presence of 0.5% BSA, which stabilizes both FFAs and glycerol by preventing their degradation (Fig. 2C). In this condition, FFAs were released at similar level between SCAds and rBMAds. In contrast, glycerol release was significantly lower in rBMAds compared to SCAds. These SCAds exhibited a FFA:glycerol ratio of ~3:1, consistent with complete TG hydrolysis, while rBMAds showed a strikingly elevated ratio of ~25:1, indicating substantial FFA release uncoupled from glycerol liberation (Fig. 2D). Given that rBMAds contain over 90% of TG[18,19], the observed FFA release is likely derived from TG hydrolysis. rBMAds express Adipose Triglyceride Lipase (ATGL), the first enzyme in the lipolytic cascade[19]. Mice with BMAd-specific deletion of ATGL, show enlarged rBMAds implicating ATGL in TG breakdown[40]. Since human ATGL inhibitors are unavailable and rBMAds lack nuclei, preventing

genetic manipulation[19], we tested the effect of pan-lipase inhibitors (orlistat and paraoxon ethyl)[41–43] on FFA and glycerol release under basal and stimulated conditions. As expected, both inhibitors reduced FFA and glycerol release in SCAds under all conditions (Fig. 2E). In contrast, rBMAds showed significant reduction in FFA release with no changes in glycerol levels, reinforcing the notion of incomplete lipolysis and absence of full TG hydrolysis in these cells. In conclusion, these findings reveal that rBMAds exhibit a non-canonical lipolytic pathway, potentially implicating ATGL, characterized by selective FFA release uncoupled from glycerol liberation, distinguishing them functionally from "classical" adipocytes.

rBMAds reprogram PCa cells toward a pro-migratory and invasive phenotype

To investigate the impact of rBMAds on PCa progression, we performed RNA-seq on five matched PC3 NC and COC. Unsupervised multivariate analysis clearly partitioned the PC3 cells based on their culture condition (Fig. 3A) with the two first components explaining 39% and 20.1% of the total variance. Of the 15 686 genes, 749 were significantly upregulated and 443 were significantly downregulated in response to coculture (Fig. 3B). Gene Ontology (GO) analysis of differentially expressed genes revealed a strong enrichment in migration-associated processes among upregulated genes. Notably, pathways related to cell migration, cell adhesion, locomotion, and the regulation of locomotion were among the most significantly induced (Fig. 3C). In contrast, downregulated genes were predominantly associated with the regulation of cell population proliferation (Fig. 3C). Given the strong induction of migration-related pathways, we next assessed PC3 cell migration using Boyden chamber and scratch assay following coculture. As shown in Fig. 3D, PC3 cells previously cocultured with rBMAds exhibited enhanced migration toward serum-containing medium compared to control cells. Similarly, in the scratch assay, wound closure was significantly accelerated in PC3 COC, indicating increased migratory capacity (Fig. 3E). This pro-migratory effect was also confirmed in Du145 and LNCaP cells (Supplementary Fig. 3A-B). In addition to increased migration, coculture with rBMAds promoted invasion of PC3 cells (Fig. 3F), as well as Du145 cells, through Matrigel-coated Boyden chambers (Supplementary Fig. 3C). Consistent with these findings, cocultured PCa cells displayed a more scattered morphology and developed multiple elongated protrusions, as revealed by actin staining (Fig. 3G, Supplementary Fig. 3D) suggesting that an epithelial mesenchymal transition (EMT) program takes place, as already demonstrated in many cancer cell models cocultivated with adipocytes[16]. Finally, we did not observe any significant changes in cell number or BrdU incorporation after 72 hours of coculture in PC3 cells (Fig. 3H, 3I), nor in other PCa cell lines (Du145 and LNCaP) (Supplementary Fig. 3E-F).

Taken together, these results showed that rBMAds promote migration and invasion of PCa cells suggesting that these adipocytes actively contribute to metastatic dissemination within the bone microenvironment leading to the polymetastatic nature of late-stage disease.

Adipocyte-derived FFAs drive PCa cell motility

Our results highlight that changes in the transcriptional landscape are key to the observed increase in motility induced by coculture, as all the most upregulated pathways were related to cell migration. Since FFAs act as regulators of gene expression that impact tumor progression[44], we first investigated whether these lipids were involved in the increased migration observed. Conditioned medium (CM) was prepared from rBMAds, and lipids were removed using lipid removal reagent. FFA quantification confirmed a significant reduction in lipid content in the delipidated CM (dCM) compared to the untreated CM (Fig. 4A). To assess the functional impact of lipid depletion, PC3 cells were treated with either CM or dCM, and intracellular lipid accumulation was evaluated. Bodipy staining showed a clear reduction in LDs in PC3 cells exposed to dCM (Fig. 4B), which was further supported by a decrease in TG content (Fig. 4C). Boyden chamber assays demonstrated that CM increased PC3 cell migration (consistent with coculture experiments), whereas this effect was lost when cells were exposed to dCM (Fig. 4D).

To further evaluate the contribution of FFAs, PC3 cells were treated for 72 hours with palmitate, oleate, or linoleate, the most abundant FFAs released by rBMAds (as shown in Fig. 1E). Exogenous FFA treatment led to neutral lipid accumulation (Fig. 4E) and increased cell motility in both Boyden chamber assays (Fig. 4F) and scratch assays (Fig. 4G). Similarly, FFA treatment enhanced migration of Du145 and LNCaP cells in the Boyden chamber assay (Supplementary Fig.4A-B). In addition, exogenous FFA treatment increase invasion of PC3 (Fig 4H). These findings demonstrate that FFAs released by rBMAds contribute to the pro-migratory phenotype of PCa cells.

ANGPTL4 as a FFA-responsive driver of PCa cell migration

Among the top 10 most upregulated genes in the coculture condition, ANGPTL4 exhibited the highest induction, with an 80-fold increase in expression in PC3 COC compared to PC3 NC (Fig. 5A). ANGPTL4 is a glycoprotein primarily known for its role in lipid metabolism, particularly as an inhibitor of lipoprotein lipase (LPL), thereby regulating plasma TG levels[45]. ANGPTL4 has also been implicated in various cancer-related processes, including cell survival, proliferation, angiogenesis, and metastasis, acting in both autocrine and paracrine manners[46]. In most models, ANGPTL4 promotes tumor cell motility via cytoskeletal remodeling, integrin activation, and extracellular matrix (ECM) degradation[47–51]. In PCa, immunohistochemical analysis of ANGPTL4 expression in PCa tissues from radical prostatectomy (RP) showed that its expression was significantly correlated with PSA (Prostate

Specific Antigen) recurrence after treatment[52]. Interestingly, ANGPTL4 is a known target of the PPARγ transcription factor, which binds and responds to diverse lipid metabolites[45,53–55].

Based on RNA-seq results, we confirmed that PC3 COC exhibit a significant increase in ANGPTL4 mRNA levels using independent RNA extracts (Fig. 5B) as well as increased protein expression (Fig. 5C), compared to PC3 NC. Similar results were obtained in Du145 cells, which also showed increased ANGPTL4 expression after coculture (Supplementary Fig. 5A-B). As previously shown[53–56], ANGPTL4 may be secreted, and we confirmed its secretion in both PC3 (Fig. 5D) and Du145 cells after coculture (Supplementary Fig. 5C), whereas it was undetectable in rBMAds or cancer cells cultivated alone (Fig. 5D; Supplementary Fig. 5C).

To assess whether ANGPTL4 overexpression could be driven by exogenous lipids, PC3 cells were treated during 72 hours with palmitate, oleate or linoleate alone or in combination (mix FFA). This led to a significant increase in ANGPTL4 gene expression in PC3 (Fig. 5E) and Du145 cells (Supplementary Fig. 5D). Given that ANGPTL4 is regulated by PPARγ, whose activity is modulated by FFAs[53,57,58], we tested this regulatory axis. Treatment of PCa cells for 24 hours with FFAs in the presence or absence of T0070907, a PPARγ inverse agonist, showed that FFA-induced ANGPTL4 expression was completely abolished by the antagonist (Fig. 5F; Supplementary Fig. 5E). Similarly, 24h of coculture-induced ANGPTL4 expression was also blocked by PPARγ inverse agonist (Fig. 5G; Supplementary Fig. 5F).

To test whether ANGPTL4 contributes functionally to PCa migration, we silenced ANGPTL4 using siRNA prior to 24h of coculture. Silencing was confirmed at both mRNA (Fig. 5H) and protein levels (Fig. 5I-J) in PC3, as well as in Du145 cells (Supplementary Fig. 5G-I). Knockdown of ANGPTL4 in PCa cells significantly reduced migration in Boyden chamber assay (Fig. 5K, Supplementary Fig. 5J) and wound closure in scratch assay (Fig. 5L) which has been enhanced in co-culture. ANGPTL4 silencing also decreased invasion capacities of PC3 cells, reinforcing its role in motility (Fig. 5M). Finally, to confirm the role of PPARγ activity in this process, PCa cells were treated with a PPARγ inverse agonist during 24-hours coculture with rBMAds. This treatment effectively abolished the migration-promoting effect of coculture, confirming that PPARγ activity is required for the observed pro-migratory phenotype (Fig. 5N; Supplementary Fig.5K). Mechanistically, ANGPTL4 has been reported to promote migration through actin cytoskeleton remodeling and pseudopodia formation[50] and to induce an EMT-like transcriptional program[59–61]. In line with this, our transcriptomic analysis revealed that coculture of PC3 with rBMAds increases EMT associated genes (Table 1) as CDH2 (Cadherin-2 encoding for N-cadherin), VIM (Vimentin) and ZEB1 (Zinc finger E-box binding homeobox 1) together with a downregulation of CDH1 (Cadherin-1 encoding for E-cadherin). Moreover, genes previously implicated in EMT in pancreatic cancer cells overexpressing ANGPTL4[62]

including ITGB4 (Integrin subunit beta 4), HBEGF (Heparin-binding EGF-like growth factor) or VEGFA (Vascular Endothelial Growth Factor A), were also upregulated in our RNA-seq (Table 1), further supporting the role of ANGPTL4 in the acquisition of migratory phenotype.

Collectively, our findings identify ANGPTL4 as a critical FFA-responsive effector that mediates PCa cell migration in response to adipocyte-derived lipid signals. Herein, we show that ANGPTL4 expression is robustly induced in cocultured PCa cells and this effect is driven by FFAs and depends on PPARγ activity. Most importantly, functional experiments using siRNA-mediated knockdown clearly demonstrate that downregulation of ANGPTL4 significantly impairs the adipocyte-driven migration and invasion of PCa cells. These results establish a direct functional link between ANGPTL4 expression and tumor cell motility. Thus, ANGPTL4 is not only a marker of lipid-induced transcriptional reprogramming but also a key driver of the migratory phenotype in PCa.

High expression of ANGPTL4 could contribute to poor overall survival in PCa patients with bone metastases

To assess the clinical relevance of our findings, we examined available datasets, although annotated collections of bone metastases remain scarce. In clinical practice, typical metastatic lesions in patients with known PCa are seldom biopsied, as diagnosis relies on clinical history, PSA levels and imaging[63] and treatment of advanced PCa rarely depends on the histology of individual bone lesions. Furthermore, PCa bone metastases are often sclerotic and yield few viable tumor cells, limiting diagnostic recovery. Despite these constraints, analysis of a clinically informative dataset[37] of 26 bone metastasis cases revealed that high ANGPTL4 expression was associated with reduced overall survival (Fig. 6A).

Concluding remarks

Using a 3D model of primary human rBMAds, we report for the first time a metabolic crosstalk between rBMAds and PCa cells, in which FFAs are released via an unconventional lipase-dependent mechanism. These FFAs are taken up by PCa cells, triggering gene remodeling through PPARγ-dependent induction of ANGPTL4 and enhancing migration and invasion. The main finding of our study is summarized in Fig. 6B. By promoting motility and invasion, crosstalk with rBMAds may facilitate not only bone colonization and remodeling by cancer cells but also their subsequent dissemination to distant osseous and non-osseous metastatic sites, contributing to the systemic, polymetastatic nature of late-stage disease. Supporting the translational potential of these observations, preclinical studies in other cancer types show that blocking antibodies against ANGPTL4 can inhibit tumor cell colonization *in vivo*[64] and reduce EMT in 3D tumor models[65].

Collectively, these results identify ANGPTL4 as a promising target to limit the migratory and invasive properties of PCa cells, warranting validation in *in vivo* models that faithfully recapitulate successive metastatic colonization, which are currently lacking for PCa.

Figure legend

Figure 1: Transfer of FFAs is observed between rBMAds and PCa cells in a 3D Co-culture model.

A. Representative images of PC3 cultivated alone (NC) or with rBMAds (COC) during 24h, 48h or 72h. PC3 NC and COC were stained with rhodamine-phalloidin (red) for F-Actin, DAPI (blue) for nuclei and Bodipy 493/503 (green) for neutral lipids. Scale bar, 20µm. **B.** Relative abundance of free cholesterol (FC), cholesterol ester (CE) and triglycerides (TG) in PC3 NC and COC after 72 hours of culture (n=8). **C.** Representative images at 24h and 72h of culture of PC3 COC previously loaded with Bodipy FLC16 (COC FLC16, in green) or without (COC ctl). Cells were stained with rhodamine-phalloidin (red) for F-Actin and DAPI (blue) for nuclei. Scale bar, 10µm. **D.** Fluorescence intensity of Bodipy FLC16 at 24h, 48h and 72h of culture of PC3 NC or COC with rBMAds previously loaded with Bodipy FLC16 (n=3). **E.** Relative abundance of FFA species contained in culture medium of rBMAds alone (rBMAds NC), PC3 NC or PC3 COC after 72 hours of culture (n=4). **F.** Relative abundance of total FFA contained in culture medium of rBMAds alone (rBMAds NC), PC3 NC and PC3 COC after 72 hours of culture (n=4). Bar pot represent mean ± SEM, non- significant (ns), *P < 0.05, **P < 0.01, ****P < 0.0001.

Figure 2: rBMAds exhibit non canonical lipolysis with uncoupled FFA and glycerol release.

A. Scheme representing lipolysis pathway in "classical" adipocytes. TG: Triglycerides, DG: Diglycerides, MG: Monoglycerides, FFA: Free Fatty Acid, ATGL: Adipose Triglyceride Lipase, HSL: Hormone Sensitive Lipase, MAGL: Monoacylglycerol Lipase. **B.** Glycerol and FFA released by subcutaneous adipocytes (SCAds) and rBMAds at basal level (Ctl, n=10) or after 3 hours of lipolysis stimulation with 1µM isoproterenol (ISO, n=10) or 10µM Forskolin (FK, n=6). **C.** FFA and glycerol released by SCAds and rBMAds during 72h of culture in medium containing 0.5% Bovine serum albumin (BSA) (n=7). **D** Ratio of FFA/Glycerol released by SCAds and rBMAds after 72h of culture in medium containing 0.5% BSA (n=7). **E.** FFA and glycerol released by SCAds and rBMAds at basal

level or after 3 hours of treatment with 100µM orlistat or 100µM paraoxon ethyl with or without isoproterenol (ISO) stimulation (n=7). Bar plot represent mean ± SEM, ns non- significant, *P < 0.05, **P < 0.01, ***P < 0.001, ****P < 0.0001.

Figure 3: rBMAds reprogram PCa cells toward a pro-migratory and invasive phenotype.

A. Principal Component Analysis of PC3 NC and COC during 72h (n=5). **B.** Volcano plot of genes detected by RNAseq with downregulated and upregulated genes by coculture represented in blue and in red respectively. **C.** Balloon plot representing the top 10 most downregulated and upregulated Gene Ontology (GO) terms in PC3 COC. **D.** Boyden chamber assay on PC3 NC and COC after 5 days of culture (n=5). **E.** Scratch assay on PC3 NC and COC after 5 days of culture. Images at the beginning (0h) and 12h after the wound are represented. The wound was normalized to time 0, when the scratch was performed and followed during 24h (n=4). Scale bar, 100µm. **F.** Invasion assay on PC3 NC and COC after 5 days of culture (n=5). **G.** Representative images of PC3 NC and COC during 72h and stained with rhodamine-phalloidin (red) for F-Actin and DAPI (blue) for nuclei. Scale bar, 10µm. **H.** Number of PC3 NC and COC after 24h, 48h and 72h of culture (n=4). **I.** OD values of BrdU incorporated at 24h, 48h and 72h into PC3 NC and COC (n=3). Bar plot and curve represent mean ± SEM, ns non- significant, **P < 0.01, ***P < 0.001, ****P < 0.0001.

Figure 4: Adipocyte-derived FFAs drive PCa cell motility.

A. FFA contained in delipidated (dCM) or control conditioned medium (CM) (n=6). **B.** Representative images of PC3 non-treated (NT) or treated with CM or dCM during 72h. Cells were stained with rhodamine-phalloidin (red) for F-Actin, DAPI (blue) for nuclei and Bodipy 493/503 (green) for neutral lipids. Scale bar, 20µm. **C.** Quantification of TG contained in PC3 NT or treated with CM or dCM during 72h (n=6). **D.** Boyden chamber assay of PC3 previously treated during 72h without (NT) or with CM or dCM (n=5). **E.** Representative images of PC3 cultivated in presence or not (ctl) of exogenous free fatty acid (FFA): palmitate, oleate, linoleate or the mix of the three-fatty acid (mix FFA). Cells were stained with rhodamine-phalloidin (red) for F-Actin, DAPI (blue) for nuclei and Bodipy 493/503 (green) for neutral lipids. Scale bar, 20µm. **F.** Boyden chamber assay of PC3 previously treated or not with palmitate, oleate, linoleate or the mix FFA for 72h (n=5). **G.** Scratch assay of PC3 previously treated or not with palmitate, oleate, linoleate or the mix FFA for 72h. The wound was normalized to time 0, when the scratch was performed and followed during 24h (n=5). **H.** Invasion assay of PC3 previously treated or not with palmitate, oleate, linoleate or the mix FFA for 72h (n=3). Bar pot and curve represent mean ± SEM, ns non-significant, *P < 0.05, **P < 0.01, ***P < 0.001, ****P < 0.0001.

Figure 5: ANGPTL4 as a FFA-responsive driver of PCa cell migration.

A. Fold change of the top 10 most upregulated genes induced by coculture in PC3 and identified by RNAseq. **B**. mRNA expression of ANGPTL4 in PC3 NC and COC after 72h of culture (n=3). **C**. Intracellular level of ANGPTL4 in PC3 NC and COC after 72h of culture (n=4). **D**. Quantification of ANGPTL4 contained in the medium of rBMAds NC, PC3 NC and PC3 COC (n=4). **E**. mRNA expression of ANGPTL4 in PC3 after 72h of treatment with exogenous FFA: palmitate, oleate, linoleate or mix of FFA or without treatment (ctl) (n=6). **F**. mRNA expression of ANGPTL4 in PC3 treated 24h with exogenous FFA in presence or in absence of PPARγ inverse agonist (10μM T0070907) (n=8). **G**. mRNA expression of ANGPTL4 in PC3 NC and COC during 24h in presence or in absence (non-treated, NT) of PPARγ inverse agonist (10μM T0070907) (n=6). **H**. mRNA expression of ANGPTL4 in PC3 NC and COC transfected with siRNA control (siCT) or with siRNA against ANGPTL4 (siANGPTL4) and after 24h of coculture (n=3). **I**. Intracellular level of ANGPTL4 in PC3 NC and COC transfected with control siCT or siANGPTL4 and after 24h of culture (n=6). **J**. Quantification of ANGPTL4 contained in the medium of PC3 NC and COC transfected with siCT or siANGPTL4 and after 24h of culture (n=6). **K**. Boyden chamber assay of PC3 NC and COC transfected with siCT or siANGPTL4 (n=5). **L**. Scratch assay on PC3 NC and PC3 COC transfected with siCT or siANGPTL4 was performed after 24h of culture. The wound was normalized to time 0, when the scratch was performed and followed during 24h (n=5). **M**. Invasion assay of PC3 NC and COC transfected with siCT or siANGPTL4 (n=4). **N**. Boyden chamber assay of PC3 NC and COC treated or not during 24h with PPARγ inverse agonist (10μM T0070907) (n=4). Bar pot and curve represent mean ± SEM, ns non-significant, *P < 0.05, **P < 0.01, ***P < 0.001, ****P < 0.0001.

Figure 6: High expression of ANGPTL4 could contribute to poor overall survival in PCa patients with bone metastases.

A. Overall survival curve of bone metastasis PCa patients with low and high level of ANGPTL4 expression. *P < 0.05. **B**. Proposed model of how rBMAds participate to tumor progression. At the bone metastatic site, PCa cells come into contact with rBMAds where a metabolic crosstalk occurs. rBMAds release FFAs via a non-conventional mechanism, independent of lipolysis pathway. These FFAs are taken up by PCa cells, and induce gene remodeling via PPARγ-dependent induction of ANGPTL4 and promotes migration and invasion properties of PCa cells. Through this mechanism, rBMAds may promote the development of polymetastatic disease by facilitating the establishment of multiple metastatic sites in the same organ or in different organs (brain, lung, liver, spine, pelvis).

Supplementary Figure legends

Supplementary figure 1: Development of 3D culture model of rBMAds.

A. Maximum intensity projection of Z-stack acquired through confocal microscopy. Representative images of rBMAds embedded in fibrin gels and stained with Bodipy 493/503 (green), after their isolation (Day 0) or after 3 days (Day 3) or 5 days of culture (Day 5). Scale bar, 100μm. **B.** Distribution of rBMAds diameter (μm) at Day 0, Day 3 and Day 5 of culture (n=9 paired samples) and the mean diameter (μm) of rBMAds. **C**. Quantification of adiponectin released by rBMAds at Day 1, Day 2 and Day 3 of culture (n=4). Bars represent mean ± SEM, ns non-significant.

Supplementary figure 2: A transfer of FFA is observed between rBMAds and PCa cells in a 3D Co-culture model.

A. Representative images of PC3, Du145 and LNCaP cultivated alone (NC) or with rBMAds (COC) at 72h of culture. Cells were stained with rhodamine-phalloidin (red) for F-Actin, DAPI (blue) for nuclei and Bodipy 493/503 (green) for neutral lipids. Scale bar, 20μm. **B.** Quantification of triglycerides (TGs) contained in PC3, Du145 and LNCaP NC and COC (n=4 PC3, n=5 Du145, LNCaP). Bar plot represent mean ± SEM, **P < 0.01, ***P < 0.001.

Supplementary figure 3: rBMAds reprogram PCa cells toward a pro-migratory and invasive phenotype.

A. Boyden chamber assay of Du145 NC and COC (n=5). **B**. Boyden chamber assay of LNCaP NC and COC (n=6). **C**. Invasion assay for 24h of LNCaP NC and COC (n=5). **D**. Representative images of Du145 NC and COC during 72h and stained with rhodamine-phalloidin (red) for F-Actin, and DAPI (blue) for nuclei. Scale bar, 20μm. **E**. Number of Du145 NC and COC after 24h, 48h or 72h of culture (n=4) **F**. Number of LNCaP NC and LNCaP COC after 24h, 48h, or 72h of culture (n=5). Bar plot represent mean ± SEM, ns non- significant, **P < 0.01.

Supplementary figure 4: Adipocyte-derived FFAs drive PCa cell motility.

A. Boyden chamber assay of Du145 previously treated or not (ctl) with palmitate, oleate, linoleate or the mix of FFA for 72h (n=6). **B**. Boyden chamber assay of LNCaP previously treated or not (ctl) with palmitate, oleate, linoleate or the mix of FFA for 72h (n=7). Bar pot represent mean ± SEM, **P < 0.01, ***P < 0.001, ****P < 0.0001.

Supplementary figure 5: ANGPTL4 as a FFA-responsive driver of PCa cell migration.

A. mRNA expression of ANGPTL4 in Du145 NC and COC, after 72h of culture (n=3). **B**. Intracellular level of ANGPTL4 in Du145 NC and COC, after 72h of culture (n=4). **C**. Quantification of ANGPTL4 contained in the medium of rBMAds cultivated alone (rBMAds), Du145 NC and Du145 COC (n=3). **D**. mRNA expression of ANGPTL4 in Du145 after 72h of treatment of exogenous FFA: palmitate, oleate, linoleate or mix of FFA or without treatment (ctl) (n=5). **E**. mRNA expression of ANGPTL4 in Du145 treated 24h with exogenous FFA in presence or in absence of PPARγ inverse agonist (10μM T0070907) (n=7). **F**. mRNA expression of ANGPTL4 in Du145 NC and COC during 24h in presence or in absence (non-treated, NT) of PPARγ inverse agonist (10μM T0070907) (n=3). **G**. mRNA expression of ANGPTL4 Du145 NC and COC transfected with siRNA control (siCT) or with siRNA against ANGPTL4 (siANGPTL4) (n=4). **H**. Intracellular level of ANGPTL4 in Du145 NC and COC, transfected with siCT or siANGPLT4 and after 24h of culture (n=5). **I**. Quantification of ANGPTL4 contained in the medium of Du145 NC and COC transfected with siCT or siANGPTL4 and after 24h of culture (n=5). **J**. Boyden chamber assay of Du145 NC and COC and transfected with siCT or siANGPTL4 (n=5). **K**. Boyden chamber assay of Du145 NC and COC treated or not during 24h with PPARγ inverse agonist (10μM T0070907). (n=5). Bar pot represent mean ± SEM, ns non-significant, *P < 0.05, **P < 0.01, ***P < 0.001, ****P < 0.0001.

Table 1 : Differential expression of EMT-related genes in PC3 cells cocultivated with rBMAds. List of EMT–associated genes, including gene IDs, that are upregulated (UP) or downregulated (DOWN) in PC3 COC. Fold change (FC) values and adjusted p-values are represented. Data obtained from RNA-seq analysis.

Acknowledgements

This study was supported by the French National Cancer Institute (INCA PLBio 2020-2024) and the *Ligue Nationale contre le Cancer* (équipe labélisée). Marine Hernandez received a PhD fellowship from French ministry of higher education and research and from the *Ligue Nationale contre le Cancer*. Sauyeun Shin received a post-doctoral fellowship from INCa PLBio (2020-28). Alessandro Taccini received a European PhD fellowship (MSCA-2022-DN-01; PROSTAMET # 101120283). This work benefited from the TRI *(Toulouse Réseau Imagerie*) imaging facility, member of the national infrastructure France-BioImaging supported by the French National Research Agency (ANR-10-INBS-04). Lipidomic analysis were performed at MetaToul (Toulouse metabolomics & fluxomics facilities, www.mth-metatoul.com on the site dedicated to Lipids Analysis Inserm I2MC) and was supported by the MetaboHUB infrastructure funded by the Agence Nationale de la Recherche under the France

2030 program (MetaboHUB ANR-11-INBS-0010; MetEx+ ANR-21-ESRE-0035; MetaboHUB (JVCE) ANR-24-INBS-0012). We thank Carine Valle from Genomics and Transcriptomics platform and Clementine Decamps from Bioinformatics platform, Technological cluster of the Cancer Research Center of Toulouse (INSERM-UMR1037) for the analysis of the transcriptional study. We are grateful to the genotoul bioinformatics platform Toulouse Occitanie (Bioinfo Genotoul, https://doi.org/10.15454/1.5572369328961167E12) for providing computing resources used for alignment.

Author contributions

N.R set up the conditions for harvesting BMAT and SCAT in close collaboration with CA and CM and supervised the samples collection. MM handled the BMAT and SCAT. MH performed most of the experiments with the help of SS and AT. CV performed RNA-seq experiment. DR analyzed RNAseq data and prepared the related figures. SD performed and prepared the figures of the imaging experiments. JBM and NG conducted lipidomic analysis. MH, CM and CA wrote the manuscript. CA and CM conceived the idea for this project and CA supervised the study.

Data availability

RNA sequencing data generated in this publication (PC3 cocultivated or not with rBMAds) have been deposited in NCBI's Gene Expression Omnibus and are accessible through GEO Series accession number GSE312982 (https://www.ncbi.nlm.nih.gov/geo/query/acc.cgi?acc=GSE312982).

Competing interests

The authors declare no competing interests.

References

1. Bergengren O, Pekala KR, Matsoukas K, Fainberg J, Mungovan SF, Bratt O, et al. 2022 Update on Prostate Cancer Epidemiology and Risk Factors—A Systematic Review. Eur Urol. 2023 Aug;84(2):191–206.

2. Wang L, Lu B, He M, Wang Y, Wang Z, Du L. Prostate Cancer Incidence and Mortality: Global Status and Temporal Trends in 89 Countries From 2000 to 2019. Front Public Health. 2022 Feb 16;10:811044.

3. Antonarakis ES, Feng Z, Trock BJ, Humphreys EB, Carducci MA, Partin AW, et al. The natural history of metastatic progression in men with prostate-specific antigen recurrence after radical prostatectomy: long-term follow-up. BJU Int. 2012 Jan;109(1):32–9.

4. Bubendorf L, Schöpfer A, Wagner U, Sauter G, Moch H, Willi N, et al. Metastatic patterns of prostate cancer: an autopsy study of 1,589 patients. Hum Pathol. 2000 May;31(5):578–83.

5. Gandaglia G, Abdollah F, Schiffmann J, Trudeau V, Shariat SF, Kim SP, et al. Distribution of metastatic sites in patients with prostate cancer: A population-based analysis. The Prostate. 2014 Feb;74(2):210–6.

6. Riihimäki M, Thomsen H, Sundquist K, Sundquist J, Hemminki K. Clinical landscape of cancer metastases. Cancer Med. 2018 Oct 16;7(11):5534–42.

7. Kang J, La Manna F, Bonollo F, Sampson N, Alberts IL, Mingels C, et al. Tumor microenvironment mechanisms and bone metastatic disease progression of prostate cancer. Cancer Lett. 2022 Apr 1;530:156–69.

8. Zhang X. Interactions between cancer cells and bone microenvironment promote bone metastasis in prostate cancer. Cancer Commun Lond Engl. 2019 Nov 21;39(1):76.

9. Hernandez M, Shin S, Muller C, Attané C. The role of bone marrow adipocytes in cancer progression: the impact of obesity. Cancer Metastasis Rev [Internet]. 2022 Jun 16; Available from: https://doi.org/10.1007/s10555-022-10042-6

10. Zhang X, Tian L, Majumdar A, Scheller EL. Function and Regulation of Bone Marrow Adipose Tissue in Health and Disease: State of the Field and Clinical Considerations. Compr Physiol. 2024 Jun 27;14(3):5521–79.

11. Roumiguié M, Estève D, Manceau C, Toulet A, Gilleron J, Belles C, et al. Periprostatic Adipose Tissue Displays a Chronic Hypoxic State that Limits Its Expandability. Am J Pathol. 2022 Jun;192(6):926–42.

12. Estève D, Roumiguié M, Manceau C, Milhas D, Muller C. Periprostatic adipose tissue: A heavy player in prostate cancer progression. Curr Opin Endocr Metab Res. 2020 Feb 1;10:29–35.

13. Laurent V, Guérard A, Mazerolles C, Le Gonidec S, Toulet A, Nieto L, et al. Periprostatic adipocytes act as a driving force for prostate cancer progression in obesity. Nat Commun. 2016 Jan 12;7:10230.

14. Laurent V, Toulet A, Attané C, Milhas D, Dauvillier S, Zaidi F, et al. Periprostatic Adipose Tissue Favors Prostate Cancer Cell Invasion in an Obesity-Dependent Manner: Role of Oxidative Stress. Mol Cancer Res MCR. 2019 Mar;17(3):821–35.

15. Zechner R. FAT FLUX: enzymes, regulators, and pathophysiology of intracellular lipolysis. EMBO Mol Med. 2015 Apr;7(4):359–62.

16. Attané C, Muller C. Drilling for Oil: Tumor-Surrounding Adipocytes Fueling Cancer. Trends Cancer. 2020 Jul;6(7):593–604.

17. Attané C, Estève D, Moutahir M, Reina N, Muller C. A protocol for human bone marrow adipocyte isolation and purification. STAR Protoc. 2021 Sep 17;2(3):100629.

18. Attané C, Estève D, Chaoui K, Iacovoni JS, Corre J, Moutahir M, et al. Human Bone Marrow Is Comprised of Adipocytes with Specific Lipid Metabolism. Cell Rep. 2020 Jan 28;30(4):949-958.e6.

19. Shin S, Hernandez M, Dauvillier S, Ducoux-Petit M, Mouton-Barbosa E, Esteve D, et al. Red bone marrow hosts metabolically active anucleate adipocytes that support hematopoiesis [Internet]. bioRxiv; 2025 [cited 2025 Dec 5]. p. 2025.12.02.691590. Available from: https://www.biorxiv.org/content/10.64898/2025.12.02.691590v1

20. Dobashi M, Kouguchi D, Kanetsuna Y, Ishii J. Histopathology of castration-resistant prostate cancer confirms changes in bone metastasis during radium-223 treatment: A case report. Urol Case Rep. 2020 Sep;32:101230.

21. Boyd AL, Reid JC, Salci KR, Aslostovar L, Benoit YD, Shapovalova Z, et al. Acute myeloid leukaemia disrupts endogenous myelo-erythropoiesis by compromising the adipocyte bone marrow niche. Nat Cell Biol. 2017 Nov;19(11):1336–47.

22. Gazi E, Gardner P, Lockyer NP, Hart CA, Brown MD, Clarke NW. Direct evidence of lipid translocation between adipocytes and prostate cancer cells with imaging FTIR microspectroscopy. J Lipid Res. 2007 Aug;48(8):1846–56.

23. Herroon MK, Diedrich JD, Rajagurubandara E, Martin C, Maddipati KR, Kim S, et al. Prostate Tumor Cell-Derived IL1β Induces an Inflammatory Phenotype in Bone Marrow Adipocytes and Reduces Sensitivity to Docetaxel via Lipolysis-Dependent Mechanisms. Mol Cancer Res MCR. 2019 Dec;17(12):2508–21.

24. Diedrich JD, Rajagurubandara E, Herroon MK, Mahapatra G, Hüttemann M, Podgorski I. Bone marrow adipocytes promote the Warburg phenotype in metastatic prostate tumors *via* HIF-1α activation. Oncotarget. 2016 Oct 4;7(40):64854–77.

25. Herroon MK, Rajagurubandara E, Hardaway AL, Powell K, Turchick A, Feldmann D, et al. Bone marrow adipocytes promote tumor growth in bone via FABP4-dependent mechanisms. Oncotarget. 2013 Nov 30;4(11):2108–23.

26. Lucas S, Tencerova M, von der Weid B, Andersen TL, Attané C, Behler-Janbeck F, et al. Guidelines for Biobanking of Bone Marrow Adipose Tissue and Related Cell Types: Report of the Biobanking Working Group of the International Bone Marrow Adiposity Society. Front Endocrinol. 2021 Sep 27;12:744527.

27. Guérard A, Laurent V, Fromont G, Estève D, Gilhodes J, Bonnelye E, et al. The Chemokine Receptor CCR3 Is Potentially Involved in the Homing of Prostate Cancer Cells to Bone: Implication of Bone-Marrow Adipocytes. Int J Mol Sci. 2021 Feb 17;22(4):1994.

28. Rebeaud M, Bouche C, Dauvillier S, Attané C, Arellano C, Vaysse C, et al. A novel 3D culture model for human primary mammary adipocytes to study their metabolic crosstalk with breast cancer in lean and obese conditions. Sci Rep. 2023 Mar 22;13(1):4707.

29. Bligh EG, Dyer WJ. A rapid method of total lipid extraction and purification. Can J Biochem Physiol. 1959 Aug;37(8):911–7.

30. Langmead B, Salzberg SL. Fast gapped-read alignment with Bowtie 2. Nat Methods. 2012 Apr;9(4):357–9.

31. Li B, Dewey CN. RSEM: accurate transcript quantification from RNA-Seq data with or without a reference genome. BMC Bioinformatics. 2011 Aug 4;12(1):323.

32. R Core Team. R: A Language and Environment for Statistical Computing [Internet]. Vienna, Austria: R Foundation for Statistical Computing; 2024. Available from: https://www.R-project.org/

33. RStudio Team. RStudio: Integrated Development for R [Internet]. Boston, MA: RStudio, PBC; 2020. Available from: https://www.rstudio.com/

34. Wickham H, Averick M, Bryan J, Chang W, McGowan LD, François R, et al. Welcome to the Tidyverse. J Open Source Softw. 2019 Nov 21;4(43):1686.

35. Chen Y, Chen L, Lun ATL, Baldoni PL, Smyth GK. edgeR v4: powerful differential analysis of sequencing data with expanded functionality and improved support for small counts and larger datasets. Nucleic Acids Res. 2025 Jan 11;53(2):gkaf018.

36. Xu S, Hu E, Cai Y, Xie Z, Luo X, Zhan L, et al. Using clusterProfiler to characterize multiomics data. Nat Protoc. 2024 Nov;19(11):3292–320.

37. Abida W, Cyrta J, Heller G, Prandi D, Armenia J, Coleman I, et al. Genomic correlates of clinical outcome in advanced prostate cancer. Proc Natl Acad Sci U S A. 2019 Jun 4;116(23):11428–36.

38. Clement E, Lazar I, Attané C, Carrié L, Dauvillier S, Ducoux-Petit M, et al. Adipocyte extracellular vesicles carry enzymes and fatty acids that stimulate mitochondrial metabolism and remodeling in tumor cells. EMBO J. 2020 Feb 3;39(3):e102525.

39. Hodson L, Skeaff CM, Fielding BA. Fatty acid composition of adipose tissue and blood in humans and its use as a biomarker of dietary intake. Prog Lipid Res. 2008 Sep;47(5):348–80.

40. Li Z, Bowers E, Zhu J, Yu H, Hardij J, Bagchi DP, et al. Lipolysis of bone marrow adipocytes is required to fuel bone and the marrow niche during energy deficits. eLife. 2022 Jun 22;11:e78496.

41. Guerciolini R. Mode of action of orlistat. Int J Obes Relat Metab Disord J Int Assoc Study Obes. 1997 Jun;21 Suppl 3:S12-23.

42. Carrière F, Renou C, Ransac S, Lopez V, De Caro J, Ferrato F, et al. Inhibition of gastrointestinal lipolysis by Orlistat during digestion of test meals in healthy volunteers. Am J Physiol Gastrointest Liver Physiol. 2001 Jul;281(1):G16-28.

43. Crow JA, Bittles V, Herring KL, Borazjani A, Potter PM, Ross MK. Inhibition of recombinant human carboxylesterase 1 and 2 and monoacylglycerol lipase by chlorpyrifos oxon, paraoxon and methyl paraoxon. Toxicol Appl Pharmacol. 2012 Jan 1;258(1):145–50.

44. Corn KC, Windham MA, Rafat M. Lipids in the tumor microenvironment: From cancer progression to treatment. Prog Lipid Res. 2020 Nov;80:101055.

45. La Paglia L, Listì A, Caruso S, Amodeo V, Passiglia F, Bazan V, et al. Potential Role of ANGPTL4 in the Cross Talk between Metabolism and Cancer through PPAR Signaling Pathway. PPAR Res. 2017;2017:8187235.

46. Tan MJ, Teo Z, Sng MK, Zhu P, Tan NS. Emerging roles of angiopoietin-like 4 in human cancer. Mol Cancer Res MCR. 2012 Jun;10(6):677–88.

47. Hefni E, Menon D, Ma T, Asiedu EB, Sultan A, Meiller T, et al. Angiopoietin-like 4 induces head and neck squamous cell carcinoma cell migration through the NRP1/ABL1/PXN pathway. Cell Signal. 2023 Aug;108:110697.

48. Huang Z, Xie J, Lin S, Li S, Huang Z, Wang Y, et al. The downregulation of ANGPTL4 inhibits the migration and proliferation of tongue squamous cell carcinoma. Arch Oral Biol. 2016 Nov;71:144–9.

49. Zhang T, Kastrenopoulou A, Larrouture Q, Athanasou NA, Knowles HJ. Angiopoietin-like 4 promotes osteosarcoma cell proliferation and migration and stimulates osteoclastogenesis. BMC Cancer. 2018 May 8;18(1):536.

50. Huang XF, Han J, Hu XT, He C. Mechanisms involved in biological behavior changes associated with Angptl4 expression in colon cancer cell lines. Oncol Rep. 2012 May;27(5):1541–7.

51. Liao YH, Chiang KH, Shieh JM, Huang CR, Shen CJ, Huang WC, et al. Epidermal growth factor-induced ANGPTL4 enhances anoikis resistance and tumour metastasis in head and neck squamous cell carcinoma. Oncogene. 2017 Apr 20;36(16):2228–42.

52. Hata S, Nomura T, Iwasaki K, Sato R, Yamasaki M, Sato F, et al. Hypoxia-induced angiopoietin-like protein 4 as a clinical biomarker and treatment target for human prostate cancer. Oncol Rep. 2017 Jul;38(1):120–8.

53. Alex S, Lange K, Amolo T, Grinstead JS, Haakonsson AK, Szalowska E, et al. Short-chain fatty acids stimulate angiopoietin-like 4 synthesis in human colon adenocarcinoma cells by activating peroxisome proliferator-activated receptor γ. Mol Cell Biol. 2013 Apr;33(7):1303–16.

54. Liu L, Zhuang X, Jiang M, Guan F, Fu Q, Lin J. ANGPTL4 mediates the protective role of PPARγ activators in the pathogenesis of preeclampsia. Cell Death Dis. 2017 Sep 21;8(9):e3054.

55. Gomes D, Sobolewski C, Conzelmann S, Schaer T, Lefai E, Alfaiate D, et al. ANGPTL4 is a potential driver of HCV-induced peripheral insulin resistance. Sci Rep. 2023 Apr 25;13(1):6767.

56. Chaube B, Citrin KM, Sahraei M, Singh AK, de Urturi DS, Ding W, et al. Suppression of angiopoietin-like 4 reprograms endothelial cell metabolism and inhibits angiogenesis. Nat Commun. 2023 Dec 12;14(1):8251.

57. Kliewer SA, Sundseth SS, Jones SA, Brown PJ, Wisely GB, Koble CS, et al. Fatty acids and eicosanoids regulate gene expression through direct interactions with peroxisome proliferator-activated receptors alpha and gamma. Proc Natl Acad Sci U S A. 1997 Apr 29;94(9):4318–23.

58. Xu HE, Lambert MH, Montana VG, Parks DJ, Blanchard SG, Brown PJ, et al. Molecular recognition of fatty acids by peroxisome proliferator-activated receptors. Mol Cell. 1999 Mar;3(3):397–403.

59. Teo Z, Sng MK, Chan JSK, Lim MMK, Li Y, Li L, et al. Elevation of adenylate energy charge by angiopoietin-like 4 enhances epithelial-mesenchymal transition by inducing 14-3-3γ expression. Oncogene. 2017 Nov 16;36(46):6408–19.

60. Shen CJ, Chang KY, Lin BW, Lin WT, Su CM, Tsai JP, et al. Oleic acid-induced NOX4 is dependent on ANGPTL4 expression to promote human colorectal cancer metastasis. Theranostics. 2020;10(16):7083–99.

61. Zhu X, Guo X, Wu S, Wei L. ANGPTL4 Correlates with NSCLC Progression and Regulates Epithelial-Mesenchymal Transition via ERK Pathway. Lung. 2016 Aug;194(4):637–46.

62. Gordon ER, Wright CA, James M, Cooper SJ. Transcriptomic and functional analysis of ANGPTL4 overexpression in pancreatic cancer nominates targets that reverse chemoresistance. BMC Cancer. 2023 Jun 8;23(1):524.

63. Archer Goode E, Wang N, Munkley J. Prostate cancer bone metastases biology and clinical management (Review). Oncol Lett. 2023 Apr;25(4):163.

64. Bajwa P, Kordylewicz K, Bilecz A, Lastra RR, Wroblewski K, Rinkevich Y, et al. Cancer-associated mesothelial cell-derived ANGPTL4 and STC1 promote the early steps of ovarian cancer metastasis. JCI Insight. 2023 Mar 22;8(6):e163019.

65. Liao Z, Lim JJH, Lee JXT, Chua D, Vos MIG, Yip YS, et al. Attenuating Epithelial-to-Mesenchymal Transition in Cancer through Angiopoietin-Like 4 Inhibition in a 3D Tumor Microenvironment Model. Adv Healthc Mater. 2024 Apr;13(10):e2303481.

Figure 1:

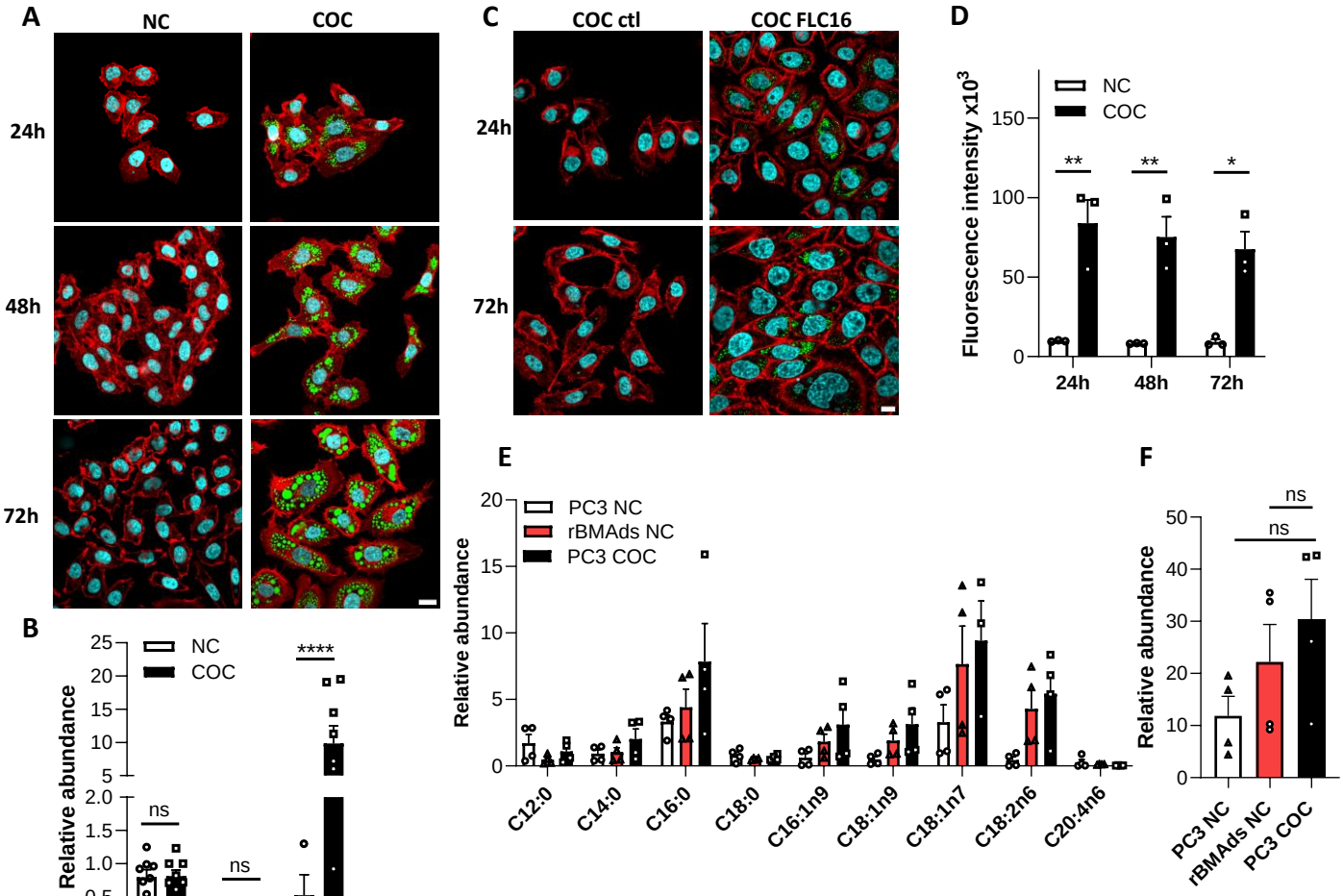
A
NC
COC
24h
48h
72h
C
COC ctl
COC FLC16
24h
72h
D
NC
COC
Fluorescence intensity x10^3
150
100
50
0
**
**
*
24h
48h
72h
B
NC
COC
Relative abundance
25
20
15
10
5
2.0
1.5
1.0
0.5
0.0
ns
ns
****
FC
CE
TG
E
PC3 NC
rBMAds NC
PC3 COC
Relative abundance
20
15
10
5
0
C12:0
C14:0
C16:0
C18:0
C16:1n9
C18:1n9
C18:1n7
C18:2n6
C20:4n6
F
ns
ns
Relative abundance
50
40
30
20
10
0
PC3 NC
rBMAds NC
PC3 COC

Figure 2 :

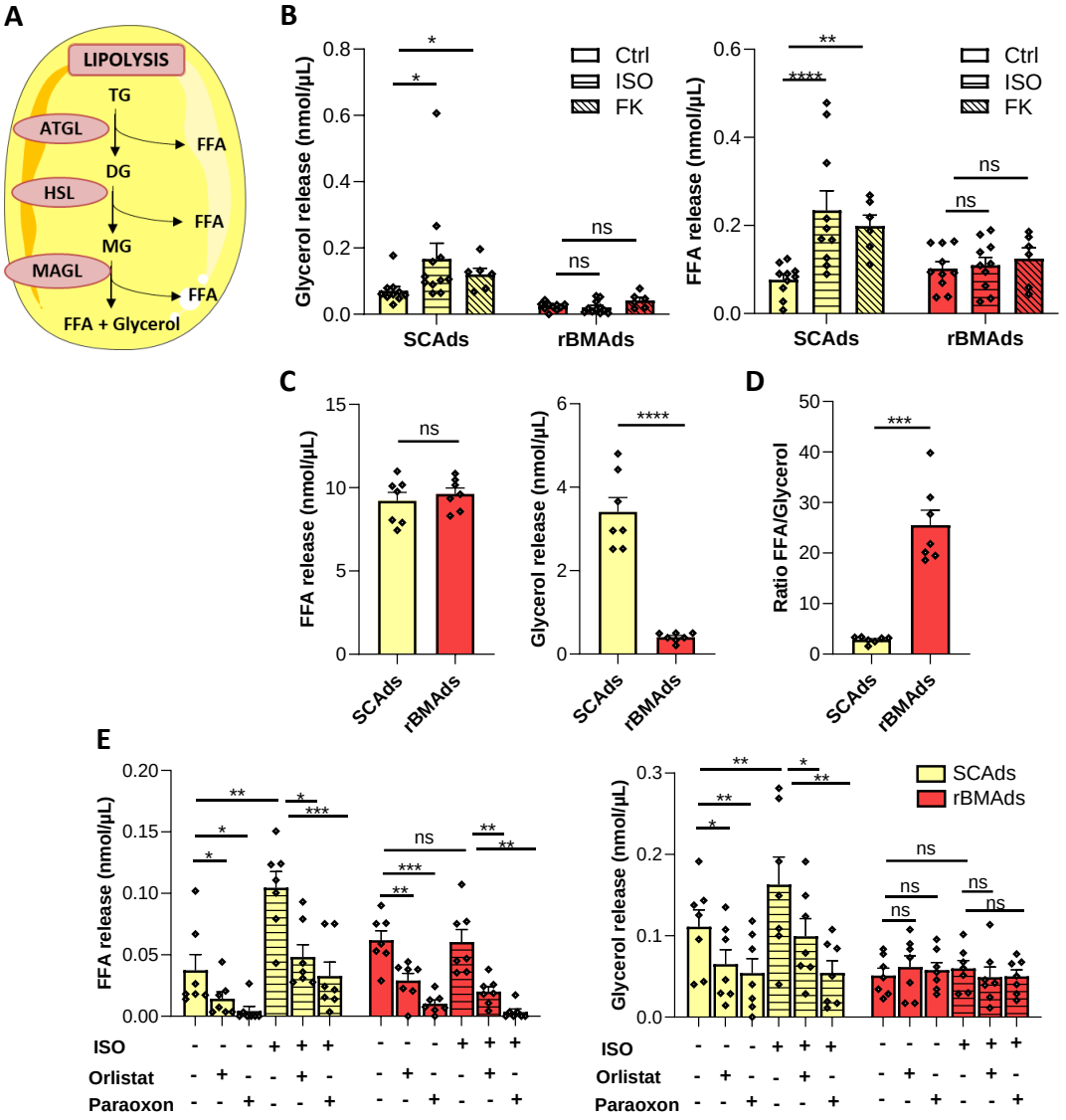
A
LIPOLYSIS
TG
ATGL
FFA
DG
HSL
FFA
MG
MAGL
FFA
FFA + Glycerol
B
Glycerol release (nmol/µL)
Ctrl
ISO
FK
SCAds
rBMAds
FFA release (nmol/µL)
C
FFA release (nmol/µL)
Glycerol release (nmol/µL)
D
Ratio FFA/Glycerol
E
FFA release (nmol/µL)
Glycerol release (nmol/µL)
SCAds
rBMAds
ISO
Orlistat
Paraoxon

Figure 3 :

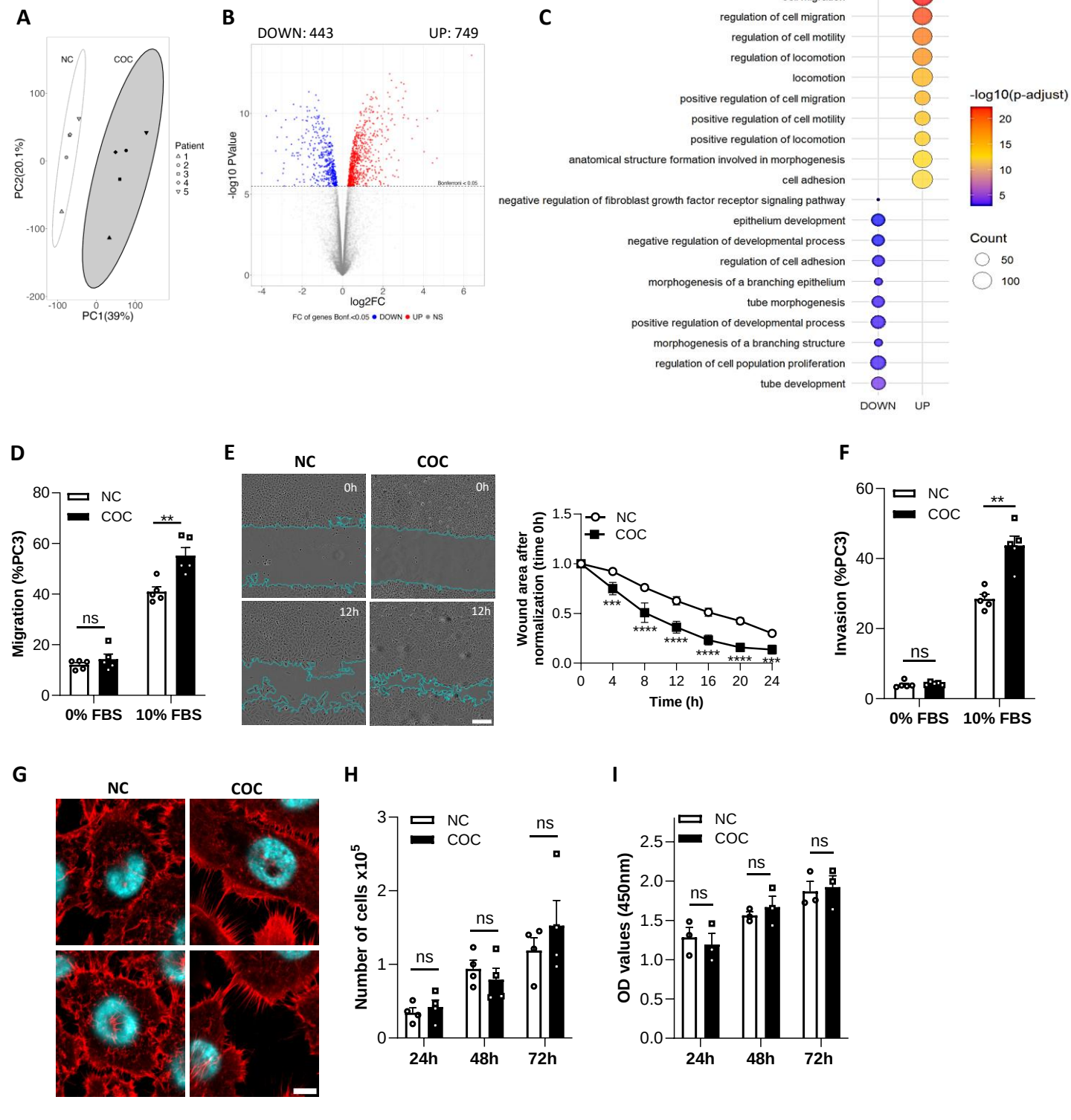
A
NC
COC
PC2(20.1%)
PC1(39%)
Patient
1
2
3
4
5
B
DOWN: 443
UP: 749
-log10 PValue
log2FC
FC of genes Bonf.<0.05 DOWN UP NS
C
TOP 10 GO terms
cell migration
regulation of cell migration
regulation of cell motility
regulation of locomotion
locomotion
positive regulation of cell migration
positive regulation of cell motility
positive regulation of locomotion
anatomical structure formation involved in morphogenesis
cell adhesion
negative regulation of fibroblast growth factor receptor signaling pathway
epithelium development
negative regulation of developmental process
regulation of cell adhesion
morphogenesis of a branching epithelium
tube morphogenesis
positive regulation of developmental process
morphogenesis of a branching structure
regulation of cell population proliferation
tube development
DOWN
UP
-log10(p-adjust)
Count
D
Migration (%PC3)
NC
COC
ns
**
0% FBS
10% FBS
E
NC
COC
0h
12h
Wound area after normalization (time 0h)
Time (h)
***
****
F
Invasion (%PC3)
G
H
Number of cells x10^5
24h
48h
72h
I
OD values (450nm)

Figure 4:

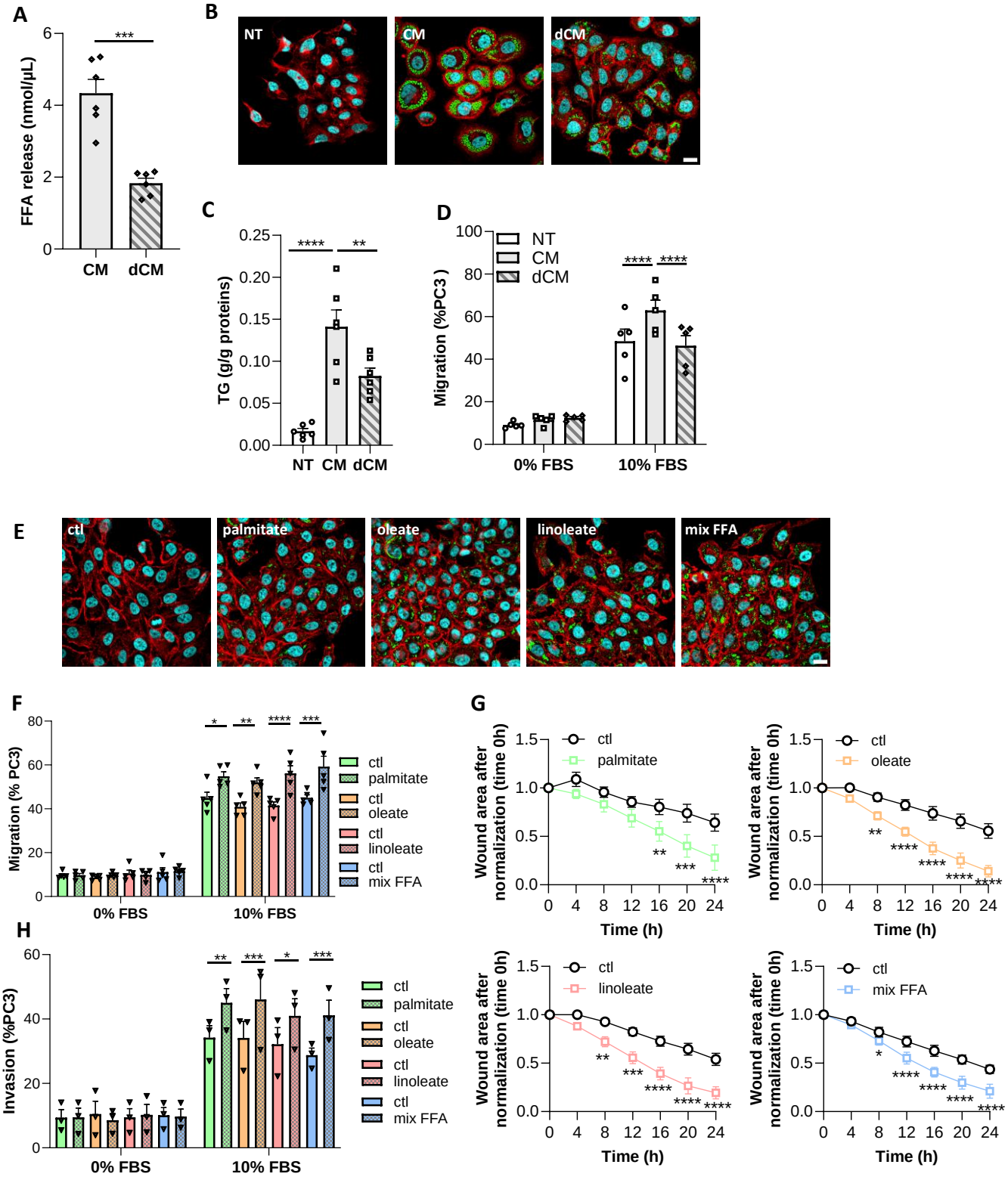
A
FFA release (nmol/µL)
CM
dCM
B
NT
CM
dCM
C
TG (g/g proteins)
NT CM dCM
D
Migration (%PC3)
NT
CM
dCM
0% FBS
10% FBS
E
ctl
palmitate
oleate
linoleate
mix FFA
F
Migration (% PC3)
0% FBS
10% FBS
G
Wound area after normalization (time 0h)
Time (h)
H
Invasion (%PC3)

Figure 5:

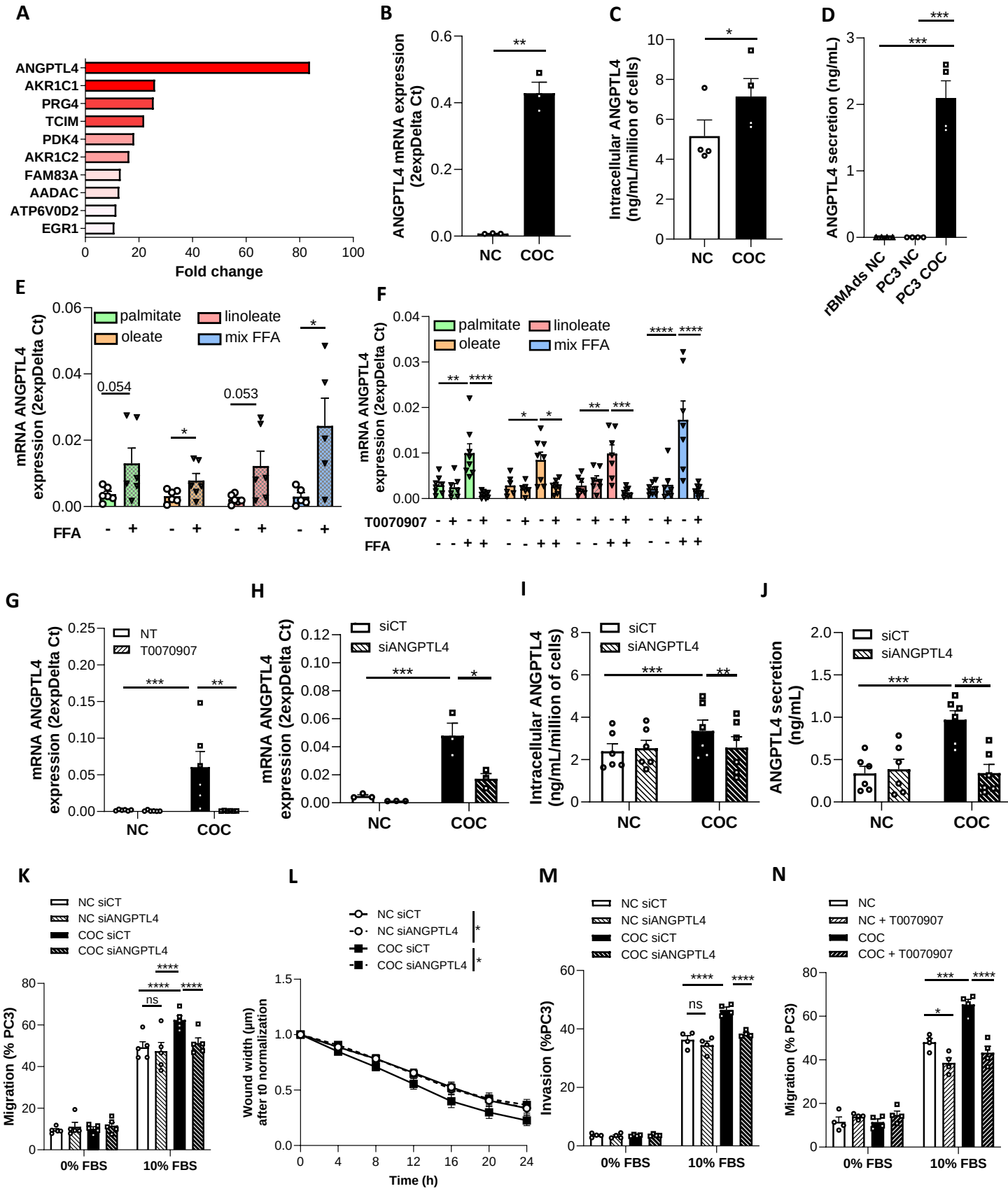
A
ANGPTL4
AKR1C1
PRG4
TCIM
PDK4
AKR1C2
FAM83A
AADAC
ATP6V0D2
EGR1
Fold change
B
ANGPTL4 mRNA expression (2expDelta Ct)
NC
COC
C
Intracellular ANGPTL4 (ng/mL/million of cells)
NC
COC
D
ANGPTL4 secretion (ng/mL)
rBMAds NC
PC3 NC
PC3 COC
E
mRNA ANGPTL4 expression (2expDelta Ct)
palmitate
oleate
linoleate
mix FFA
0.054
0.053
FFA
F
mRNA ANGPTL4 expression (2expDelta Ct)
palmitate
oleate
linoleate
mix FFA
T0070907
FFA
G
mRNA ANGPTL4 expression (2expDelta Ct)
NT
T0070907
NC
COC
H
mRNA ANGPTL4 expression (2expDelta Ct)
siCT
siANGPTL4
NC
COC
I
Intracellular ANGPTL4 (ng/mL/million of cells)
siCT
siANGPTL4
NC
COC
J
ANGPTL4 secretion (ng/mL)
siCT
siANGPTL4
NC
COC
K
NC siCT
NC siANGPTL4
COC siCT
COC siANGPTL4
Migration (% PC3)
ns
0% FBS
10% FBS
L
NC siCT
NC siANGPTL4
COC siCT
COC siANGPTL4
Wound width (µm) after t0 normalization
Time (h)
M
NC siCT
NC siANGPTL4
COC siCT
COC siANGPTL4
Invasion (%PC3)
ns
0% FBS
10% FBS
N
NC
NC + T0070907
COC
COC + T0070907
Migration (% PC3)
0% FBS
10% FBS

Table 1 : **Differential expression of EMT-related genes in PC3 cells cocultivated with rBMAds.**

Gene name	Ensembl gene ID	Fold change	Regulation	Adjusted p-value
CDH1	ENSG00000039068	-1,61	DOWN	4,20E-04
CDH2	ENSG00000170558	1,27	UP	1,90E-05
VIM	ENSG00000026025	1,09	UP	3,80E-02
ZEB1	ENSG00000148516	1,34	UP	2,37E-05
ITGB4	ENSG00000132470	1,22	UP	6,75E-04
HBEGF	ENSG00000113070	1,75	UP	2,00E-06
VEGFA	ENSG00000112715	1,45	UP	1,98E-05